Tumor Imaging Using a Standardized Radiolabeled Adapter Protein Docked to Vascular Endothelial Growth Factor

Francis G. Blankenberg, MD[1,2]; Stefanie Mandl, PhD[1]; Yu-An Cao, PhD[1]; Caitlin O'Connell-Rodwell, PhD[1]; Christopher Contag, PhD[1]; Carina Mari, PhD[2]; Timur I. Gaynutdinov, PhD[3]; Jean-Luc Vanderheyden, PhD[4]; Marina V. Backer, PhD[3]; and Joseph M. Backer, PhD[3]

[1]*Department of Pediatrics, Stanford University, Stanford, California;* [2]*Division of Nuclear Medicine, Department of Radiology, Stanford University, Stanford, California;* [3]*SibTech, Inc., Newington, Connecticut; and* [4]*Theseus Imaging Corporation, Boston, Massachusetts*

Direct radiolabeling of proteins can result in the loss of targeting activity, requires highly customized procedures, and yields heterogeneous products. Here we describe a novel imaging complex comprised of a standardized ^{99m}Tc-radiolabeled adapter protein noncovalently bound to a "Docking tag" fused to a "Targeting protein". The assembly of this complex is based on interactions between human 109-amino acid (HuS) and 15-amino acid (Hu-tag) fragments of ribonuclease I, which serve as an "Adapter protein" and a Docking tag, respectively. **Methods:** HuS modified with hydrazinonicotinamide (HYNIC) was radiolabeled using ^{99m}Tc-tricine to a specific activity of 3.4–7.4 MBq/μg. Protein complexes were then formed by mixing ^{99m}Tc-HuS with equimolar amounts of either Hu-tagged VEGF$_{121}$ (Hu-VEGF [vascular endothelial growth factor]) or Hu-tagged anti-VEGFR-2 single-chain antibody (Hu-P4G7) and incubating on ice for 15 min. 4T1 *luc/gfp* luciferase-expressing murine mammary adenocarcinoma cells (1×10^4) were implanted subcutaneously or injected intravenously into BALB/c mice. Bioluminescent imaging (BLI) was performed 10 d later. Immediately after BLI visualization of tumor, 18.5–37 MBq of tracer (5–10 μg of protein) were injected via tail vein. One hour later planar or SPECT images were obtained, followed by killing the mice. **Results:** There was significantly ($P = 0.0128$) increased uptake of ^{99m}Tc-HuS/Hu-VEGF ($n = 10$) within subcutaneous tumor as compared with ^{99m}Tc-HuS/Hu-P4G7 ($n = 5$) at biodistribution assay (2.68 ± 0.75 vs. 1.8 ± 0.21; tumor-to-subcutaneous tissue [ratio of specific activities], respectively), despite similar molecular weights. The focal ^{99m}Tc-HuS/Hu-VEGF uptake seen on planar images (3.44 ± 1.16 [tumor to soft-tissue background]) corresponded directly to the locations of tumor observed by BLI. Region of interest analyses of SPECT images revealed a significant increase of ^{99m}Tc-HuS/Hu-VEGF ($n = 5$) within the lungs with BLI-detectable pulmonary tumor nodules as compared with controls ($n = 4$) (right: 4.47 ± 2.07 vs. 1.79 ± 0.56; left: 3.66 ± 1.65 vs. 1.62 ± 0.45, tumor lung [counts/pixel]/normal lung [counts/pixel], respectively). **Conclusion:** ^{99m}Tc-HuS/Hu-VEGF complex is stable for at least 1 h in vivo and can be effectively used to image mouse tumor neovasculature in lesions as small as several millimeters in soft tissue. We expect that a similar approach can be adapted for in vivo delivery of other targeting proteins of interest without affecting their bioactivity.

Key Words: vascular endothelial growth factor; radionuclide imaging; protein complexes; ribonuclease I; SPECT

J Nucl Med 2004; 45:1373–1380

A growing number of cell-surface markers have been found that are associated with the onset and progression of cancer. Some of these markers, such as growth factor receptors, are direct targets for experimental therapeutics (*1,2*). Therefore, molecules such as growth factors and antibodies that recognize these markers are of potential interest as imaging agents. Importantly, the imaging of multiple markers in the same patient presents unique opportunities for development of personalized treatment regiments and rational selection of patients for experimental therapeutics. However, lack of efficient technology for "loading" imaging agents onto proteins prevents a widespread use of targeted imaging.

Here we describe simple and effective procedure for using assembled targeting complexes for radionuclide imaging of tumor vasculature. This system is based on an adapter/docking tag system set of interactions between 2 fragments of human ribonuclease I (RNase I) known as HuS and Hu-tag (*3*). We have fused Hu-tag complementary DNA (cDNA) to the cDNA of the circulating 121-amino acid isoform of vascular endothelial growth factor VEGF$_{121}$ and expressed the resultant fusion protein product, Hu-tagged-VEGF$_{121}$ (Hu-VEGF). We then tested the complex of ^{99m}Tc-HuS/Hu-VEGF in vitro and in vivo as an imaging reagent to detect VEGFR-2 expression, a cell-surface receptor that is overexpressed on endothelial cells at sites of pathologic angiogenesis (*4,5*). With ^{99m}Tc-HuS/Hu-VEGF complex we

Received Nov. 19, 2003; revision accepted Feb. 5, 2004.

For correspondence or reprints contact: Francis G. Blankenberg, MD, Department of Pediatrics, Stanford University, Stanford, CA 94304.
E-mail: blankenb@stanford.edu

FIGURE 1. Assembly of complexes for radionuclide imaging. Docking tag (Hu-tag) shown in light blue is fused to Targeting protein (purple) without affecting its binding epitopes (shown in yellow). Radionuclide chelator hydrazinonicotinamide is conjugated to HuS Adapter protein and loaded with ^{99m}Tc as marked by arrows. Hu-tagged Targeting protein can then bind specifically to complementary component of ^{99m}Tc-HuS and form a protein complex that also has RNase I activity.

have been able to image implants of the 4T1 murine adenocarcinoma cell line in both the subcutaneous tissues and the lungs. This nondestructive approach to the labeling of delicate proteins such as VEGF could be therefore an important step in characterization of tumors and in assessing the efficacy of various anticancer therapies, particularly those targeting angiogenesis.

MATERIALS AND METHODS

Engineering of 4T1 *luc/gfp* Murine Mammary Adenocarcinoma Cells

Virus collection and cell infection of murine mammary adenocarcinoma 4T1 cells were conducted as previously described (*6*). These cells were transduced with a retrovirus (pMSCV/L2G) encoding a dual reporter gene for the expression of both firefly luciferase and green fluorescent protein. Briefly, the open reading frame (ORF) of the firefly luciferase gene was amplified by polymerase chain reaction from pGL3-Basic (Promega). This product was then fused in frame to the ORF of the enhanced green fluorescent protein (EGFP) with 54 base pairs (bp) of the foot-and-mouth disease virus (FMDV) 2A sequence followed by 24 bp of polylinker (intervening sequence between the 2 ORFs): CAGAACTTTGACCTGCTCAAGTTGGCTGGAGATGTGG-AGTCCAACCCTGGGCCCGGGATCCACCGGCCGGTC-GCCACC). The FMDV 2A sequence serves as a ribosomal slippage site to allow the expression of the second reporter gene (EGFP). This dual reporter gene cassette was then cloned into retroviral vector pMSCV (Clontech) and the resulting construct, pMSCV/L2G, was transfected into PT67 packaging cells.

4T1 Murine Tumor Models

Female BALB/c mice were obtained from the breeding facility of the Department of Comparative Medicine, Stanford University. All mice were used between 6 and 12 wk of age. Care of all experimental animals was in accordance with institutional guidelines and approved protocols and the animals were housed and treated in a humane manner in strict accordance with Department of Agriculture and institutional animal subjects guidelines (National Institutes of Health publication No. 86-23, revised 1985). 4T1 *luc/gfp* luciferase-expressing murine mammary adenocarcinoma cells (1×10^4) were implanted subcutaneously or injected intravenously via tail vein into BALB/c mice to generate subcutaneous or pulmonary tumor nodules, respectively. Ten days after tumor inoculation, both subcutaneous and lung tumor-bearing mice under went bioluminescent imaging (BLI) and radionuclide imaging.

Generation of Recombinant Tagged Fusion Proteins

A diagram of the assembly of targeting imaging complexes consisting of standardized "Adapter protein" and a fusion "Targeting protein" expressed with a corresponding "Docking tag" is shown in Figure 1. The Docking tag shown in blue represents the 1- to 15-amino acid fragment of human RNase I (Hu-tag). The cDNA fragment of Hu-tag was fused to the cDNA of $VEGF_{121}$ or Hu-p4G7, a single-chain anti-VEGFR-2 single-chain antibody. The parental P4G7 single-chain antibody fusion protein has a molecular weight and affinity to VEGFR-2 close to that of the $VEGF_{121}$ fusion protein dimer but is not internalized on binding to VEGFR-2 (*7*). We chose to construct and use Hu-p4G7 fusion protein to separate the effects of binding and internalization of our radiolabeled imaging complexes in vivo. The plasmid with cDNA for the parental single-chain antibody P4G7 was generously provided by ImClone Systems Inc.

The cDNAs of Hu-tagged $VEGF_{121}$ (Hu-VEGF) and Hu-tagged anti-VEGFR-2 single-chain antibody (Hu-P4G7) were then expressed, purified from inclusion bodies, and refolded into functionally active conformations as described elsewhere (*3*). The fusion protein is labeled as Targeting protein as is shown in purple in Figure 1. Following convention, we will refer to the dimer of Hu-tagged $VEGF_{121}$ (a dimer with a calculated molecular weight of 33,058 with a 2-tag linker of 7 amino acids contributing 5,110 to the overall molecular weight) as "Hu-VEGF" throughout the rest of this article. The Hu-p4G7 antibody fusion protein constructed for this study is a monomer with a calculated molecular weight of 30,535 with a single tag linker of 16 amino acids contributing 3,513 to the overall molecular weight.

The 18- to 127-amino acid fragment of RNase I, named HuS, shown in yellow in Figure 1 (also known as the Adapter protein) was constructed from cDNA, which was then expressed and purified as described elsewhere (*3*). HuS was then subsequently modified with hydrazinonicotinamide (HYNIC) shown as dots indicated by arrows on the surface of the HuS protein to permit the binding of ^{99m}Tc for radiolabeling. Binding of HuS to Hu-VEGF or Hu-p4G7 also led to the full reconstitution of native RNase I

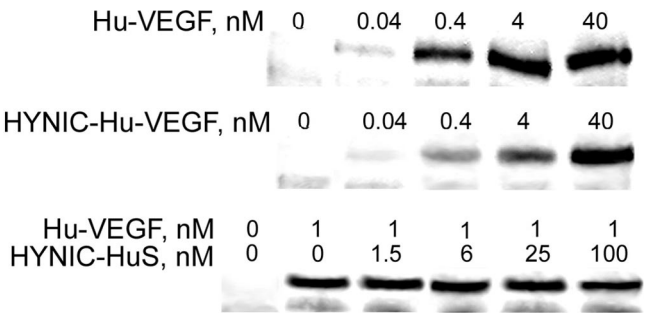

FIGURE 2. Conjugation of HYNIC to Hu-VEGF, but not docking of HYNIC-HuS, inhibits its ability to activate VEGFR-2. 293/KDR human embryonic kidney cells, engineered to express 2×10^6 molecules of VEGFR-2 per cell, were stimulated for 5 min at 37°C with increasing amounts of HYNIC-VEGF (top), Hu-VEGF (middle), or with 1 nmol/L Hu-VEGF in the presence of increasing amounts of HYNIC-HuS (bottom), then lysed and analyzed by Western blotting using antiphosphotyrosine RC20:HRPO conjugate PY (BD Bioscience). Top panel shows marked decrease in VEGFR-2–mediated tyrosine phosphorylation with modification of Hu-VEGF with HYNIC as compared with unmodified protein activity shown in middle panel. Bottom panel shows that VEGFR-2 mediated phosphorylation at a constant concentration of 1 nmol/L Hu-VEGF is unchanged by docking of increasing amounts of HYNIC-HuS.

activity, providing an excellent assay for monitoring complex formation in vitro.

The activities of Hu-VEGF, HYNIC-Hu-VEGF, and the HuS/Hu-VEGF complex were tested in an in vitro VEGFR-2 tyrosine phosphorylation assay. 293/KDR cells and assay for VEGFR-2 tyrosine phosphorylation were described previously (*2*,*3*).

Radiolabeling of Imaging Complexes

HuS and Hu-VEGF were modified with HYNIC to the molar ratio of 2:1 as described (*8*). Radiolabeling with ^{99m}Tc-tricine as a precursor complex to a specific activity of 3.7–7.4 MBq/μg protein was performed before imaging experiments (*9*). After radiolabeling of HYNIC-HuS with ^{99m}Tc using ^{99m}Tc-tricine, stable complexes with either Hu-VEGF or Hu- P4G7 were formed by gentle mixing followed by incubation of equimolar amounts tagged targeting protein and ^{99m}Tc-HYNIC-HuS on ice for 10–15 min.

Biodistribution and Clearance Studies

Two groups of normal BALB/c mice received injections of 18.5–37 MBq (5–10 μg of protein) of either ^{99m}Tc-HuS ($n = 4$) or ^{99m}Tc-HuS/Hu-VEGF ($n = 8$) via the tail vein. One hour after injection, mice were killed for biodistribution assay. Tissue and organ samples were analyzed with scintillation well counter along with 3 samples of standard activity (1/100 of injected dose) at an energy level of 140 keV and an energy window of ±20 keV. Results are expressed as the average of the percentage of injected dose per gram of tissue (%ID/g) ± 1 SD of the mean. A 1-tailed Student *t* test with an equal variance was used to calculate significance at $P < 0.05$. An additional group of 3 mice received 18.5 MBq (5 μg of protein) ^{99m}Tc-HuS/Hu-VEGF followed by serial tail vein sampling of blood activity at 1, 5, 10, 30, and 60 min after intracardiac injection of tracer.

In Vivo BLI, Planar, and SPECT Imaging

For imaging, mice were anesthetized with ketamine (100 mg/kg intraperitoneally) (Fort Dodge) and xylazine (10 mg/kg intraperitoneally) (Butler), and an aqueous solution of luciferin (150 mg/kg intraperitoneally) (Xenogen Corp.) was injected 15 min before BLI imaging. Animals were placed into the light-tight chamber of the BLI imaging system consisting of a cooled CCD (charged coupled device) camera system and the IVIS 100 camera (Xenogen Corp.). Data were presented as pseudocolor images representing light intensity (blue least and red most intense) superimposed over

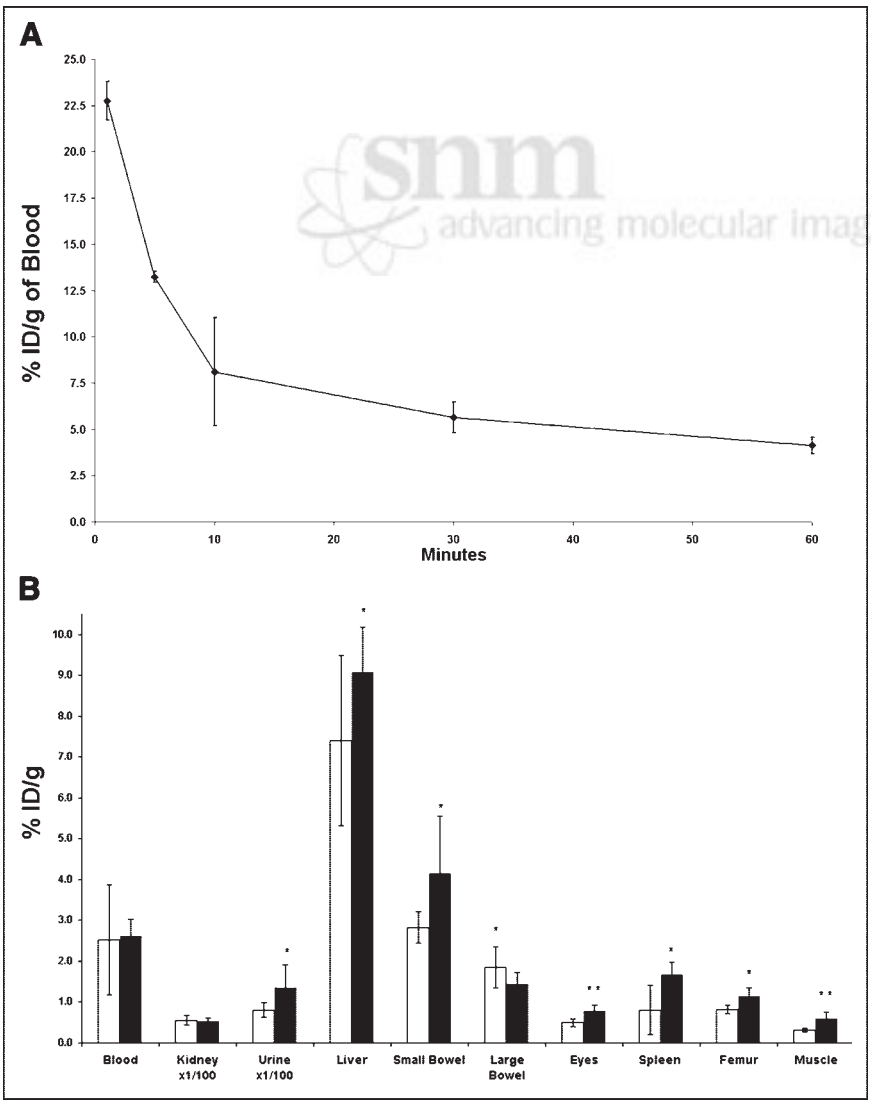

FIGURE 3. (A and B) Blood clearance and biodistribution of ^{99m}Tc-HuS/VEGF complex. (A) Three normal mice received intracardiac injection of 18.5 MBq ^{99m}Tc-HuS/VEGF complex at time zero. Tail vein blood was then obtained serially at 1, 5, 10, 30, and 60 min after injection of tracer. Results are expressed as %ID/g of blood. (B) Two additional groups of mice received tail vein injections of 18.5–37 MBq of either ^{99m}Tc-HuS/VEGF complex (■, $n = 8$) or ^{99m}Tc-HuS (□, $n = 4$). One hour after injection, mice were killed and %ID/g of various tissues was determined. Uptake of ^{99m}Tc-HuS/VEGF complex was compared with that of ^{99m}Tc-HuS alone using Student's 1-tailed *t* test of significance. Error bars = 1 SD of mean value; $^{*}P < 0.05$; $^{**}P < 0.006$.

gray-scale reference images of the whole animal. These images were collected and processed using LivingImage (Xenogen Corp.) software as an overlay on Igor image analysis software (Wavemetrics, Inc.).

One hour before radionuclide imaging, 18.5–37 MBq ^{99m}Tc-HuS/Hu-VEGF or ^{99m}Tc-HuS/Hu-P4G7 (5–10 μg of protein) were injected via tail vein, after which 5-min posterior supine planar images of tracer activity were obtained using the A-SPECT dedicated small animal imaging SPECT γ-camera (γ-Medical Instruments). For SPECT imaging, tumor-bearing mice underwent whole-body imaging, including the chest and abdomen, using a parallel-hole, high-sensitivity collimator with a 360° rotation, 15 s per 3° step, and a 64 × 64 imaging matrix with an imaging time of approximately 13 min per animal. Data were reconstructed using commercially available software (Mirage Software, version 5.3; Segami Corp.) into a 64^3 3-dimensional imaging matrix from which 1.2-mm-thick axial slices through the chest and abdomen were extracted with a voxel size of 1.2 × 1.2 × 1.2 mm. Immediately after radionuclide imaging, mice were killed by biodistribution and autoradiographic assay. Region of interest (ROI) image analyses were performed on both planar and reconstructed axial SPECT image, again using commercially available software (Mirage Software, version 5.3; Segami Corp.). Activities from both planar and axial SPECT image analyses were expressed as counts/pixel.

Autoradiography of Soft-Tissue Tumors

Immediately after radionuclide imaging mice were killed and a section of subcutaneous tumor was removed and frozen. Histologic sections (50 μm) were obtained via a cryomicrostat and then placed on glass slides for an overnight exposure on a phosphor storage screen (Phosphoimager:SI System; Molecular Dynamics). After exposure, the phosphor screen images were read out with a laser digitizer at a resolution of 50 μm per pixel. ROI analysis of radiotracer activity was performed using Image Quant Software, version 5.1 (Molecular Dynamics).

RESULTS

In Vitro Assay of Tagged Targeting Proteins and Adapter Protein

Direct conjugation of HYNIC to Hu-VEGF inhibited its ability to bind and activate VEGFR-2, as judged by the dose dependences of VEGFR-2 tyrosine phosphorylation (Fig. 2, top and middle panels). Please note the baseline activity (bottom linear density noted at the origin of each lane) for the increasing concentrations of Hu-VEGF (middle panel) and HYNIC-Hu-VEGF (top panel). In contrast, conjugation of HYNIC to the adapter protein HuS (molar ratio of 2:1) decreased its ability to bind to Hu-VEGF only 25%–30%, as judged by a reconstituted RNase activity (data not shown). Furthermore, docking HYNIC-HuS (at increasing concentrations) to Hu-VEGF (at a constant concentration of 1 nmol/L) did not affect its ability to induce VEGFR-2 phosphorylation (Fig. 2, bottom panel).

Blood Clearance and Biodistribution Assays

Serial tail sampling at 1, 5, 10, 30, and 60 min after intracardiac injection of tracer demonstrated that ~85% of the ID of ^{99m}Tc-HuS/Hu-VEGF complex was cleared in the first 10 min, as shown in Figure 3A. Furthermore, there was a bimodal exponential decrease of injected tracer composed of a fast first component with a half-life of 6.1 ± 2.2 min ($n = 3$), followed, at 10 min, by a slower second component with a half-life of 62.1 ± 22.4 min ($n = 3$).

The biodistribution of ^{99m}Tc-HuS/Hu-VEGF complex and ^{99m}Tc-HuS at 1 h after intravenous injection revealed significantly ($P < 0.050$) increased uptake of ^{99m}Tc-HuS/Hu-VEGF complex in the liver, small bowel, eyes (retina), spleen, femur, and skeletal muscle (Fig. 3B), possibly reflecting the low level of VEGF-R2 expression found in these tissues described by prior investigators (*10*). Both tracers also showed an equally large nonspecific renal uptake (≈2 %ID) and urinary excretion (≈10 %ID) and virtually identical blood activity. There was also significantly greater uptake in the remaining carcass in mice injected with ^{99m}Tc-HuS/Hu-VEGF complex as compared with ^{99m}Tc-HuS alone (24.2 ± 3.6 %ID vs. 15.4 ± 1.92 %ID, $P = 0.0047$), presumably due to the increased uptake of the protein complex in skeletal muscle. Scintillation well counting also revealed that <1.5% of total injected ^{99m}Tc activity for both ^{99m}Tc-HuS alone (1.48 ± 0.51 %ID) and ^{99m}Tc-HuS/Hu-VEGF complex (1.27 ± 0.25 %ID) localized to the

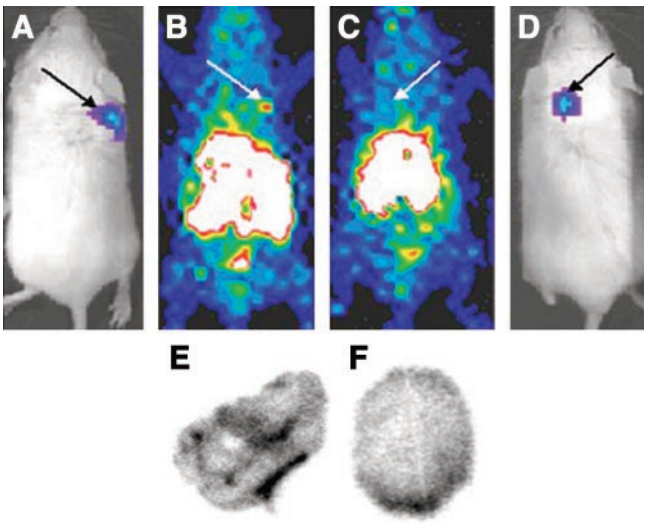

FIGURE 4. Radionuclide imaging of small subcutaneous tumors with VEGF-driven assembled complexes. Colocalization of tumors visualized by in vivo BLI and targeted radionuclide imaging. Two groups of tumor-bearing mice ($n = 5$, ^{99m}Tc-HuS/Hu-P4G7 antibody; $n = 10$, ^{99m}Tc-HuS/Hu-VEGF) were anesthetized for planar whole-body BLI and radionuclide imaging 10 d after implantation of *luc/gfp* cells into shoulder region. (A) BLI of mouse with right shoulder tumor. (B) Radionuclide image of same mouse as in A 1 h after injection of ^{99m}Tc-HuS/Hu-VEGF. (C) Radionuclide image of mouse with left shoulder tumor after injection of ^{99m}Tc-HuS/Hu-P4G7. (D) BLI of same mouse as in C. Black arrows in A and D mark tumor locations as observed by BLI. White arrows in B and C mark location of tumor on radionuclide images. Autoradiographs of frozen 50-μm histologic sections from tumors harvested 1 h after tail vein injection are shown for ^{99m}Tc-HuS/Hu-VEGF (E) and ^{99m}Tc-HuS/Hu-P4G7 (F) complexes.

stomach, suggesting little to no free ^{99m}Tc-pertechnetate in the circulation at 1 h. This implies that the protein complexes were stable in vivo with respect to the bond between ^{99m}Tc and the HYNIC moiety on the targeting proteins for at least 1 h.

Targeted Imaging of Small Subcutaneous Tumors

Tumor-bearing mice were imaged 10 d after subcutaneous implantation of 1×10^4 4T1 *luc/gfp* cells into BALB/c mice. At this time, tumors reached 2- to 3-mm maximal diameter with an average tumor volume of 18.4 ± 12.2 mm^3 ($n = 15$) and were readily visualized by BLI performed just before radionuclide imaging, as shown in Figures 4A and 4D. ^{99m}Tc-HuS/Hu-VEGF (18.5–37 MBq; $n = 10$) or ^{99m}Tc-HuS/Hu-P4G7 (18.5–37 MBq; $n = 5$) was then injected via the tail vein and 1 h later planar and SPECT radionuclide images were obtained. Intense focal uptake of ^{99m}Tc-HuS/Hu-VEGF within tumor was observed in all 10 tumor-bearing mice, as shown in Figures 4B and 4C. The sites of ^{99m}Tc-HuS/Hu-VEGF uptake directly corresponded to the locations of tumors observed by BLI. Despite comparable molecular weight and affinity to VEGFR-2, there was little visible tumor uptake of ^{99m}Tc-HuS/Hu-p4G7 (Fig. 4C). Autoradiography of excised subcutaneous tumors revealed marked heterogeneity of tracer uptake within each tumor, as shown in Figures 4E and 4F. Biodistribution assay of subcutaneous tumor revealed significantly higher uptake of ^{99m}Tc-HuS/Hu-VEGF as compared with that of ^{99m}Tc-HuS/Hu-P4G7, as shown in Figure 5: ranging from a ratio of tumor to soft-tissue background activity of 1.17 to 5.84 for ^{99m}Tc-HuS/Hu-VEGF and a ratio of tumor to soft-tissue background activity of 1.11 to 2.02 for ^{99m}Tc-HuS/Hu-P4G7. ROI analyses showed a 4- to 5-fold increase in tumor localization of ^{99m}Tc-HuS/Hu-VEGF as compared with soft-tissue background activity.

Targeted Imaging of Pulmonary Tumors

To test the utility of VEGF-driven assembled imaging complexes for detection of tumors in internal organs, we injected 4T1 *luc/gfp* cells via tail vein into mice (1×10^4 cells per mouse). Injection of tumor cells via the tail vain leads to experimental pulmonary metastasis. Ten days after tail vein injection of tumor cells, regions of pulmonary tumor were detectable by in vivo BLI ($n = 4$), as shown in Figure 6. Due to light scattering within the soft tissues, individual nodules of tumor were not distinguishable in the BLI images. However, the BLI images did reflect the amount of tumor burden within each lobe of the lung quantitatively. One hour after tail vein injection of 18.5–37 MBq ^{99m}Tc-HuS/Hu-VEGF, SPECT radionuclide imaging

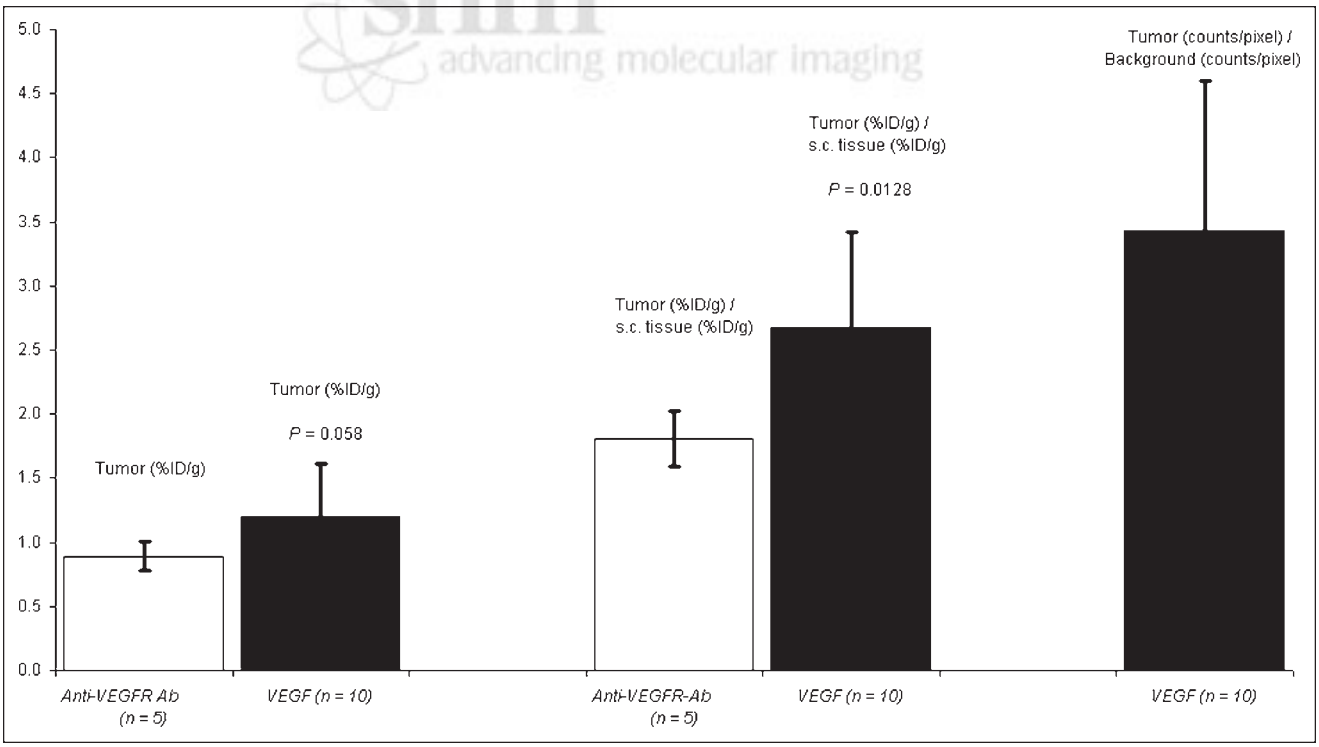

FIGURE 5. Biodistribution and ROI data analyses of subcutaneous tumor 10 d after inoculation. Bar graphs of average values of tracer uptake expressed as %ID/g and ratio of specific activity of tumor to normal soft-tissue uptake are shown for ^{99m}Tc-HuS/Hu-VEGF and ^{99m}Tc-HuS/Hu-P4G7 complexes. Ratio of tumor (counts/pixel) to normal soft-tissue (counts/pixel) uptake of ^{99m}Tc-HuS/Hu-VEGF complex were obtained by ROI analyses of planar images. Please note that subcutaneous tumor could not be seen with ^{99m}Tc-HuS/Hu-P4G7 complex; therefore, ROI analyses for this tracer were not performed. Error bars = 1 SD of mean values. *P* values comparing uptake of ^{99m}Tc-HuS/Hu-VEGF with ^{99m}Tc-HuS/Hu-P4G7 complex using a 1-tailed Student *t* test are shown. s.c. = subcutaneous.

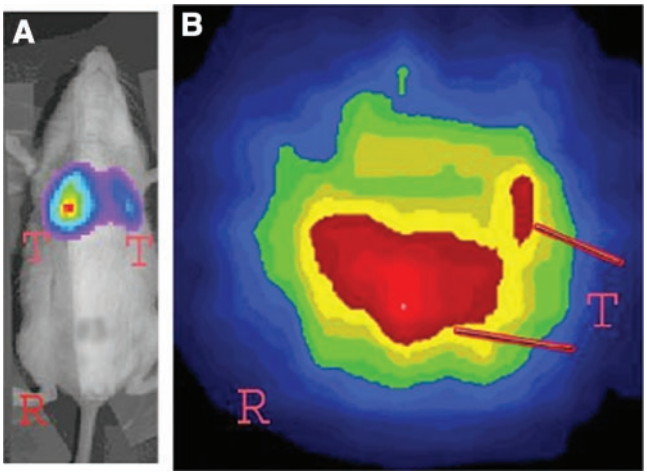

FIGURE 6. Radionuclide imaging of pulmonary tumors with VEGF-driven assembled complexes. Radionuclide SPECT images were obtained immediately after in vivo planar whole-body BLI. Please note that pulmonary tumor deposits were confluent and appeared as diffuse increases in lung luminescence or activity by BLI and SPECT, respectively. (A) Planar BLI of mouse with bilateral lung tumors. Note marked tumor burden (T) of right lung (R) as compared with left lung. (B) Transverse radionuclide SPECT tomographic slice through lungs of same mouse as in A 1 h after injection of ^{99m}Tc-HuS/VEGF. Regions of lung tumor (T) are marked by red lines on transverse tomographic slice of midchest with markedly more tracer uptake on right (R) as compared with left lung. Large region of tracer uptake in right lung was 521% greater than that of blood-pool (heart) activity; smaller region within left lung was 326% as seen by ROI image analyses.

revealed a significant presence of radioactivity in the lungs with BLI-detectable pulmonary tumor burden. ROI image and biodistribution analyses indicated that lungs from animals with pulmonary tumor had significantly greater tracer uptake than that of the lungs of mice with subcutaneous tumors but without BLI-detectable pulmonary metastasis ($n = 5$), as shown in Figure 7.

DISCUSSION

We fused Hu-tag (Docking tag) to the circulating 121-amino acid isoform of VEGF, $VEGF_{121}$. $VEGF_{121}$ was chosen as a Targeting protein because it lacks the heparin binding domain that may interfere with in vivo localization and because its main receptor, VEGFR-2, is overexpressed on endothelial cells at the sites of pathologic angiogenesis (*4,5*). We then nondestructively labeled $VEGF_{121}$ for imaging using the humanized form of Adapter protein/Docking tag system based on the noncovalent interactions between 2 fragments of the RNase I (*2,3*): HuS (Adapter protein) and Hu-tag (Docking tag). It should be noted that our human RNase I–based Adapter protein/Docking tag system evolved from a bovine RNase A system (*2*), known as S-protein and S-peptide, that was described nearly 44 y ago (*11*).

There are at least 2 other major strategies for radiolabeling proteins with ^{99m}Tc (or other isotopes) (*1,8*). In the first approach, either imaging agents or their chelators are directly conjugated to targeting proteins. In the second approach, imaging agents are loaded onto a carrier that is either conjugated to targeting proteins or bound to a specific adapter that is conjugated to the targeting proteins. Since both strategies rely on random chemical modification of targeting proteins, they share common problems, such as (a) partial inactivation of functional domains, (b) heterogeneity of final products, and (c) customized conjugation procedure for every targeting protein. These problems represent major obstacles associated with cell-specific proteins for targeted imaging. Indeed, the marked decreased ability of HYNIC-VEGF to stimulate the VEGFR-2 in vitro as compared with native VEGF or HuS/Hu-VEGF complex emphasizes the disadvantages of direct chemical modification of fragile targeting proteins as compared with assembling imaging complexes.

Our data show that ^{99m}Tc-HuS/Hu-VEGF complex, formed by nondestructive methods, can be used to image subcutaneous as well as internal tumors as small as several millimeters. Since normal vasculature is not imaged in these experiments, the high conspicuity of lesions on planar and SPECT imaging is due to the ^{99m}Tc-HuS/Hu-VEGF of tumor blood vessels that overexpress VEGFR-2 (*4,5*). This finding was confirmed by autoradiography.

VEGFR-2–mediated uptake of ^{99m}Tc-HuS/Hu-VEGF by endothelial cells may also be beneficial, since the noninternalizable anti-VEGFR-2 antibody P4G7 of similar molecular weight and binding affinity failed to image tumors under similar conditions. The failure of anti-VEGFR-2 antibody P4G7 as a tracer suggests that nonspecific uptake of imaging complexes by tumors, through enhanced permeability retention mechanism(s) (*12*) alone, is not sufficient for imaging. As VEGF is internalized shortly after binding to VEGFR-2, tumor vascular cells act as biologic sinks, gradually increasing intracellular tracer activity as compared with anti-VEGFR-2 antibody P4G7, which remains on the cell surface. Indeed, autoradiography of histologic sections also established a higher range of focal activity for tumors from animals that received ^{99m}Tc-HuS/Hu-VEGF as compared with ^{99m}Tc-HuS/Hu-P4G7, as shown in Figure 4. Intratumoral distribution of both targeting proteins was far from uniform, reflecting most likely a well-known heterogeneity of tumor vasculature (*13*).

Several alternative approaches have been advocated for the noninvasive assessment of tumor neovascularity, including anti-$\alpha_v\beta_3$ integrin antibody-coated polymerized liposomes for MRI (*14*) as well as technetium-labeled endostatin (*15*) and $\alpha_v\beta_3$ integrin binding peptides (*16*). Targeted MRI of tumor neovascularity, however, requires at least 5–10 times more targeting protein and approximately 1 million- to 1 billion-fold more contrast agent than does radionuclide-based techniques (*17*). Radiolabeled endostatin or $\alpha_v\beta_3$ integrin binding peptides may hold promise as imaging agents in the future but, as of yet, have only been able to image the neovascularity of fairly large tumors,

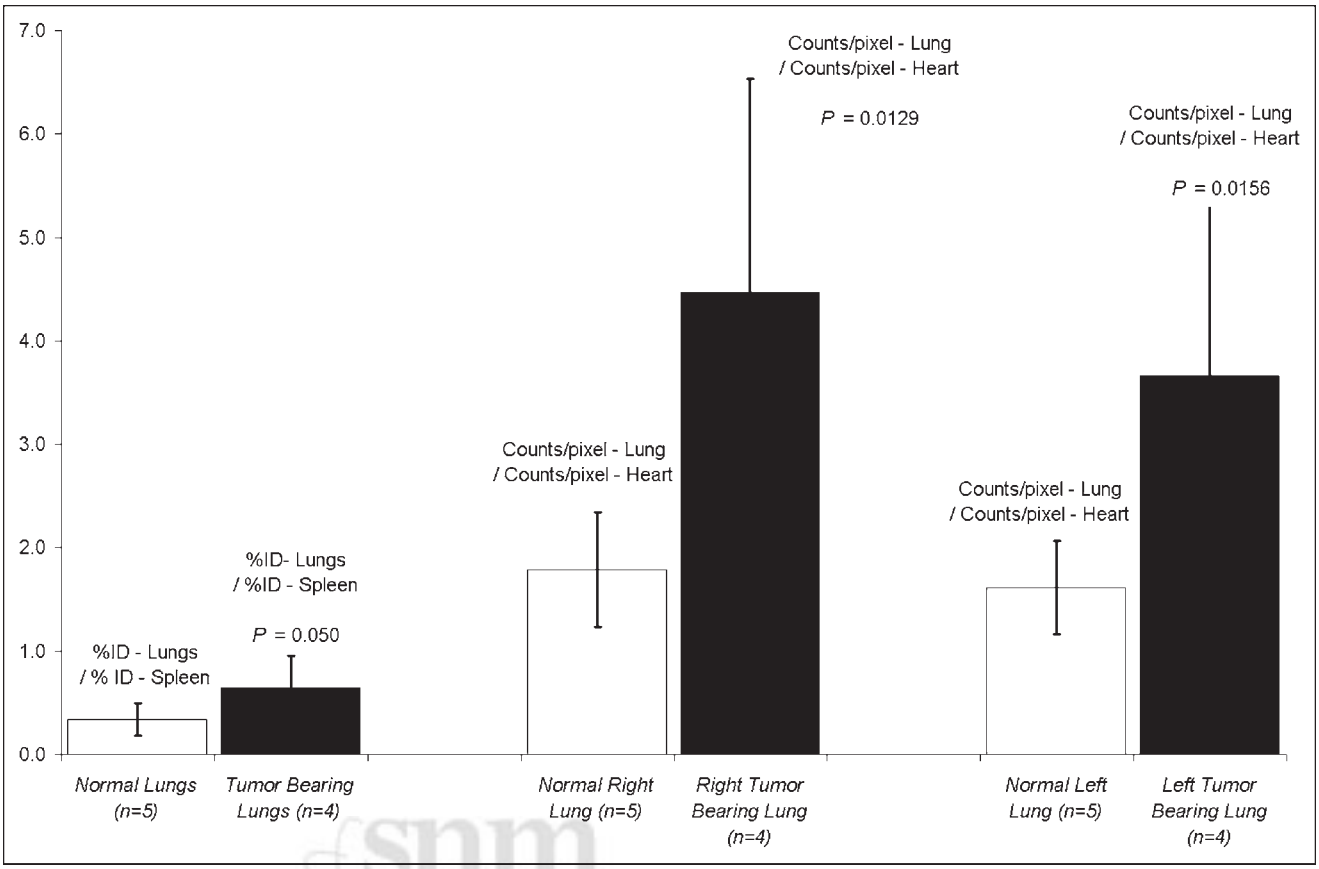

FIGURE 7. Biodistribution and ROI data analyses of pulmonary tumor. Bar graphs of average values of tracer uptake expressed as ratio of lung activity (%ID) to splenic activity (%ID) are shown for ^{99m}Tc-HuS/Hu-VEGF complex in normal (n = 5) and tumor-bearing (n = 4) lungs. Ratios of right and left lung (counts/pixel) to heart (counts/pixel) uptake of ^{99m}Tc-HuS/Hu-VEGF complex, obtained by ROI analyses of SPECT images of lungs of mice with and without tumor, are shown. Error bars = 1 SD of mean values. P values comparing uptake of ^{99m}Tc-HuS/Hu-VEGF complex in normal vs. tumor-bearing lung using 1-tailed Student t test are shown.

ranging from 5 to 10 mm in diameter in mice. The high sensitivity of ^{99m}Tc-HuS/VEGF radionuclide imaging might allow earlier detection of tumors and metastatic lesions and more effective monitoring of their responses to treatments.

We expect that ^{99m}Tc-HuS, a standardized radionuclide imaging "payload" module, can be readily used with a variety of Targeting proteins armed with the Docking tag. Further development of ^{99m}Tc-HuS, such as increasing its specific activity by using polychelating moieties, will be instrumental in application of assembled complexes to targeted imaging of multiple tumor- or patient-specific markers. To facilitate this development we have recently constructed a functionally active Adapter protein with a unique cysteine residue for a site-specific conjugation to different polymeric carriers (Backer MV, Gaynutdinov TI, Patel V, et al., unpublished data, 2004).

CONCLUSION

We propose the use of our standardized HuS-Adapter protein/Docking tag fusion protein system for targeted imaging with a variety of different protein-based radiotracers. Since the HuS-Adapter protein and Hu-tag peptide are fragments of human RNase I, they provide distinct advantages over potentially more immunogenic streptavidin-biotin–based docking systems that also require direct modification of a targeting protein or expression of a protein with a nonhuman "biotinylatable" tag (*18*). We expect that standardized payload modules can be constructed by loading contrast agents onto the HuS Adapter protein. These payload modules might be used with any targeting protein expressed with a Docking tag. On the other hand, we expect that a Targeting protein with a Docking tag might be used with different ready-to-use imaging payload modules. Experiments are now in progress to construct standardized payload modules for various imaging modalities, including MRI and PET scanning.

ACKNOWLEDGMENTS

This work was supported in part by a grant from the National Institutes of Health (2R44 HL6143-02), a grant from the Department of Army (DAMD17-03-C-0011), gift

monies and supplies for from Theseus Imaging Corporation, and support from the National Cancer Institute (R24CA92862 and P20CA86312), the Hess Research Fund, the Mary L. Johnson Research Fund, and the Bio-X Program at Stanford University.

REFERENCES

1. Dubowchik GM, Walker MA. Receptor-mediated and enzyme-dependent targeting of cytotoxic anticancer drugs. *Pharmacol Ther.* 1999;83:67–123.
2. Backer MV, Aloise R, Przekop K, Stoletov K, Backer JM. Molecular vehicles for targeted delivery. *Bioconjug Chem.* 2002;13:462–467.
3. Backer MV, Gaynutdinov TI, Gorshkova II, et al. Humanized docking system for assembly of targeting drug delivery complexes. *J Control Release.* 2003;89:499–511.
4. Brown LF, Berse B, Jackman RW, et al. Increased expression of vascular permeability factor (vascular endothelial growth factor) and its receptors in kidney and bladder carcinomas. *Am J Pathol.* 1993;143:1255–1262.
5. Brown LF, Berse B, Jackman RW, et al. Expression of vascular permeability factor (vascular endothelial growth factor) and its receptors in breast cancer. *Hum Pathol.* 1995;26:86–91.
6. Edinger M, Cao YA, Verneris MR, Bachmann MH, Contag CH, Negrin RS. Revealing lymphoma growth and the efficacy of immune cell therapies using in vivo bioluminescence imaging. *Blood.* 2003;101:640–648.
7. Lu D, Kotanides H, Jimenez X, et al. Acquired antagonistic activity of a bispecific diabody directed against two different epitopes on vascular endothelial growth factor receptor 2. *J Immunol Methods.* 1999;230:159–171.
8. Abrams MJ, Juweid M, tenKate CI. Technetium-99m-human polyclonal IgG radiolabeled via the hydrazino nicotinamide derivative for imaging focal sites of infection in rats. *J Nucl Med.* 1990;31:2022–2028.
9. Larsen SK, Solomon HF, Caldwell G, Abrams MJ. [^{99m}Tc]Tricine: a useful precursor complex for the radiolabeling of hydrazinonicotinamide protein conjugates. *Bioconjug Chem.* 1995;6:635–638.
10. Witmer AN, Dai J, Weich HA, Vrensen GFJM, Schlingemann RO. Expression of vascular endothelial growth factor receptors 1, 2, and 3 in quiescent endothelia. *J Histochem Ctyochem.* 2002;50:767–777.
11. Richards FM, Vithayathil PJ. The preparation of subtilisin-modified ribonuclease and the separation of the peptide and protein components. *J Biol Chem*. 1959; 234:1459–1465.
12. Maeda H, Wu J, Sawa T, Matsumura Y, Hori K. Tumor vascular permeability and the EPR effect in macromolecular therapeutics: a review. *J Control Release.* 2000;65:271–284.
13. Gillies RJ, Schornack PA, Secomb TW, Raghunand N. Causes and effects of heterogeneous perfusion in tumors. *Neoplasia.* 1999;1:197–207.
14. Sipkins DA, Cheresh DA, Kazemi MR, Nevin LM, Bednarski MD, Li KC. Detection of tumor angiogenesis in vivo by $\alpha_V\beta_3$-targeted magnetic resonance imaging. *Nat Med.* 1998;4:623–626.
15. Yang DJ, Kim KD, Schechter NR, et al. Assessment of the antiangiogenic effect using ^{99m}Tc-EC-endostatin. *Cancer Biother Radiopharm.* 2002;17:233–246.
16. Jassen ML, Oyen WJ, Dijkgraaf I, et al. Tumor targeting with radiolabeled $\alpha_v\beta_3$ intergrin binding peptides in a nude mouse model. *Cancer Res.* 2002;62:6146–6151.
17. Blankenberg FG, Eckelman WC, Strauss HW, et al. Role of radionuclide imaging in trials of antiangiogenic therapy. *Acad Radiol.* 2000;7:851–867.
18. Smith PA, Tripp BC, DiBlasio-Smith EA, Lu Z, LaVallie ER, McCoy JM. A plasmid expression system for quantitative in vivo biotinylation of thioredoxin fusion proteins in Escherichia coli. *Nucleic Acids Res.* 1998;26:1414–1420.